A New Method for Breast Cancer Identification Using Multi-modal Features in Quaternionic Form

G. Apostolopoulos[1], A. Koutras[2,1], I. Christoyianni[1] and E. Dermatas[1]

[1] Wired Communications Lab, Electrical and Computer Engineering Department, University of Patras, Greece
[2] Informatics and Mass Media Department, Technical Educational Institute of Western Greece, Greece

***Abstract*—Mammography is still the most effective procedure for early diagnosis of the breast cancer. Computer-aided Diagnosis (CAD) systems can be very helpful in this direction for radiologists to recognize abnormal and normal regions of interest in digital mammograms faster than traditional screening program. In this work, we propose a new method for breast cancer identification of all types of lesions in digital mammograms using multimodal features in a quaternionic representation. The proposed method consists of two steps: First, a novel feature extraction module utilizes two dimensional discrete transforms based on ART, Shapelets, Zernike moments and Gabor filters to decompose Regions of Suspicion (ROS) into a set of localized basis functions with different shapes. The extracted features are then fused and presented in quaternionic representation to the classification module in the second step. For the classification task, we propose a new type of classifier (Q-classifier) that successfully, accurately, with low computational cost and higher speed of diagnosis, recognizes normal and abnormal ROS from mammograms. The proposed method is evaluated on the Mini-MIAS database. The methods' performance is evaluated using Receiver Operating Characteristics (ROC) curve. The achieved result AUC = 0.934 shows that the proposed method can be quite effective and can be used as a tool for efficiently diagnosing breast cancer compared to similar techniques presented in the literature that use SVM classifiers and unimodal features.**

Keywords—Shapelets; ART; Zernike-Moments; Gabor-filter banks; Quaternion; Breast cancer; Computer-aided diagnosis (CAD)

I. INTRODUCTION

Breast cancer is one of the most important health problems, taking the second place between all types of cancer in the world. Specifically, in the case of women, breast cancer is the most frequent type of cancer with an estimated 1.67 mil. new cases diagnosed in 2012 (a quarter of all cancer cases) according to [1]. When breast cancer is diagnosed in the early stages through screening and diagnostic digital mammography, the treatment and survival rates in most of the cases can be significantly increased. However, early detection of suspicious abnormalities using digital mammography is prone to a high degree of human error between 10%-30% [2-3]. Of these errors, half can be attributed to misinterpretation of cancer signs, while in the rest of the cases, detection errors are due to human over-look [2]. The cost of this misinterpretation leads to unwanted and costly biopsies on the benign lesions that result to anxiety for the patient, as well as they cost money. For this reason, the development of reliable Computer Aided Diagnosis (CAD) systems that will help radiologists and minimize detection and diagnosis errors is of great importance. In order for CAD systems to work efficiently, the important task is to find and use the most suitable mammographic image descriptors that when used, will improve the recognition accuracy and discriminate normal from abnormal mammograms correctly, as well as benign / malignant in the latter case.

In the area of feature extraction and classification of mammographic tissue, several researches have been conducted and numerous scientific papers have been proposed in the literature during the last years that use different features and neural classifiers [4-11]. In this paper however, we present a new multimodal feature extraction technique based on a combination of different image decomposition methods that is capable of recognizing efficiently normal and abnormal regions of interest (ROI) of mammograms regardless their type of abnormality.

In this study, we propose a new method to classify regions of suspicion (ROS) that contain abnormal or healthy breast tissue using a multimodal feature extraction technique based on Shapelets (SH), Angular Radial Transform (ART), Zernike Moments (ZM), Gabor Filter Banks (GFB) and a new type of classifier that is based on quaternion representation. The proposed method decomposes each tested ROS into a series of localized basis functions with different shapes, which are called SH, ART, ZM and GFB. These multi-modal coefficients are then fused and form the descriptors in quaternionic representation. Extensive experiments have shown great accuracy of the proposed feature set and recognition module that exceeds 86% in the task of recognizing normal and abnormal breast tissue in digital mammograms.

The structure of this paper is as follows: In the next section, a detailed description of the multimodal set of features extracted from mammograms is given. Additionally, a description of the proposed classifier based on the quaternion representation (Q-classifier) is also given. In section 3 we present the data set and the experimental results and finally, in section 4 some conclusions are drawn.

II. THE PROPOSED CAD SYSTEM

The proposed CAD system consists of the feature extraction module that decomposes each examined ROS into a set of localized basis functions with different shapes. The robust feature sets related to the Angular Radial Transform (ART), Shapelets (SH), Zernike moments (ZM) and Gabor filters bank (GFB) are used to encode the image data. The estimated coefficients of the

ISBN 978-0-9928626-7-1

above integral transformations are fused and presented in quaternionic representation to the Classification module (Q-classifier) that performs the diagnosis of normal or abnormal region.

A. Quaternions

Quaternions were first introduced by Hamilton [12] and constitute of an extension of complex numbers. Quaternions are mainly used in computer vision problems due to their ability to represent 3D rotations easily. They are also used for the representation of color images by encoding the RGB channels into their imaginary parts [13-14]. The main advantage of quaternion-based representation is that any information stored in array structures can be totally treated as a vector. Further reading of quaternions properties can be found in [15].

B. Shapelet Transform

The Shapelet image decomposition method was first introduced in [16]. It has been used efficiently to estimate discrimination data based on several expressions of the spatial pixels' distribution of an object as a linear sum of a set of orthogonal 2D functions in various image processing problems. Therefore, in this paper we investigate the use of shapelet transform in the task of accurate detection of ROS areas (normal and abnormal). Polar shapelets [16] present all major properties of the Cartesian Shapelets with a scaling β, and in addition are also separable in ρ and θ domain. For this reason, polar shapelets coefficients are easier to comprehend in terms of rotational symmetries, simpler and more intuitive. A function $I(\rho,\theta)$ in polar coordinates is decomposed as a weighted sum:

$$I(\rho,\theta)=\sum_{n=0}^{\infty}\sum_{m=-n}^{+n} f_{n,m}\cdot x_{n,m}(\rho,\theta;\beta) \tag{1}$$

where $x_{n,m}(r,\theta;\beta)$ are the polar basis functions related to Laguerre polynomials $L_{\frac{n-|m|}{2}}^{|m|}$, and

$$x_{n,m}(\rho,\theta;\beta)=\frac{(-1)^{\frac{n-|m|}{2}}}{\beta^{|m|+1}}\cdot\left[\frac{\left[\left(n-|m|\right)/2\right]!}{\pi\left[\left(n+|m|\right)/2\right]!}\right]^{1/2}\cdot\rho^{|m|}\cdot L_{\frac{n-|m|}{2}}^{|m|}\left(\frac{\rho^2}{\beta^2}\right)\cdot e^{\frac{-\rho^2}{2\cdot\beta^2}}\cdot e^{-i\cdot m\cdot\theta} \tag{2}$$

with n and m both even or odd, respectively. The polar shapelets coefficients of order n and m are calculated using the overlap integral:

$$f_{n,m}^{SH}=\iint_{\square} I(\rho,\theta)\cdot x_{n,m}(\rho,\theta;\beta)\cdot\rho\cdot d\rho\cdot d\theta \tag{3}$$

As polar shapelets basis functions are complex numbers, the shapelets coefficients $f_{n,m}$ are complex numbers as well, for $m=0$, the basis functions have only a real part.

C. Angular Radial Transform

The Angular Radial Transform (ART) is a moment-based image description method and can be used to encode region-based information [17]. This integral transformation provides a compact and efficient expression of brightness distribution within a 2-D object region, describing both connected and disconnected region shapes. The ART is a complex orthogonal transformation defined on a unit disk that consists of the complete orthogonal sinusoidal basis functions in polar coordinates [18,19].

$$f_{n,m}^{ART}=\int_0^{2\pi}\int_0^{1} V_{n,m}(\rho,\theta)\cdot I(\rho,\theta)\cdot\rho\cdot d\rho\cdot d\theta \tag{4}$$

where $I(\rho,\theta)$ is the ROS image in polar coordinates, $V_{n,m}(\rho,\theta)$ the ART basis function that is separable along the angular and radial directions.

$$V_{n,m}(\rho,\theta)=A_m(\theta)\cdot R_n(\rho)\text{, where}$$
$$A_m(\theta)=\frac{1}{2\pi}e^{jm\theta},\ R_n(\rho)=\begin{cases}1, & n=0\\ 2\cdot\cos(\pi n\rho), & n\neq 0\end{cases} \tag{5}$$

D. Zernike Moments

The moments proposed by Frederik Zernike in 1934 [20], were used in digital image analysis problems and evaluated for many types of images [21-22]. According to Khotanzad et al. [23], Zernike moments have strong separability and can be used to identify shapes efficiently. The usage of Zernike Moments in mammography first introduced by [24].

Zernike moments are defined as a family of orthogonal functions over the unit disk. In polar coordinates the Zernike function $Z_n^m(\rho,\theta)$ is defined by:

$$Z_n^{\pm m}(\rho,\theta)=R_n^m(\rho)\cdot e^{jm\theta} \tag{6}$$

where $R_n^m(\rho)$ are the Zernike polynomials. The index n is the degree of the polynomial, while m is the polynomial order. The Zernike polynomials are defined as a finite sum of powers of ρ^2:

$$R_n^m(\rho)=\sum_{k=0}^{(n-|m|)/2}\frac{(-1)^k\cdot(n-k)!}{k!\cdot\left(\frac{n+|m|}{2}-k\right)!\cdot\left(\frac{n-|m|}{2}-k\right)!}\cdot\rho^{n-2k} \tag{7}$$

where $n=0,1,2,\cdots,\infty$ and $m=-n,-n+2,-n+4,\cdots,+n$, with $n-|m|=$ even and $|m|\leq n$. The Zernike moments are orthogonal, ensuring that there is minimum correlation among them, resulting to minimum information redundancy, invariant both to rotation and displacement.

E. Gabor-filters Bank

The spatial band-pass Gabor filters have excellent resolution in both spatial and frequency domains. Daugman et al. [25] generalized the Gabor filters in two dimensions, which can be represented as a complex sinusoidal signal modulated by a Gaussian kernel function [26]:

$$G(x,y,\theta,f)=e^{-\frac{1}{2}\left(\left(\frac{x_\theta}{\sigma_x}\right)^2+\left(\frac{y_\theta}{\sigma_y}\right)^2\right)}\cdot\cos(2\cdot\pi\cdot f\cdot x_\theta) \tag{8}$$

$x_\theta=x\cdot\cos(\theta)+y\cdot\sin(\theta)$, $y_\theta=y\cdot\cos(\theta)-x\cdot\sin(\theta)$, σ_x and σ_y are the standard deviations of the Gaussian envelope along the x and y dimensions, f is the central frequency of the

sinusoidal plane wave, and θ is the orientation. The convolution of the ROS image with each of the Gabor filters gives:

$$g_{f,\theta}(x,y) = I(x,y) ** G_{f,\theta}(x,y) \tag{9}$$

where $g_{f,\theta}$ is the output of the filter, I the ROS image, $G_{f,\theta}$ the Gabor filter and $(**)$ denotes the 2D convolution. Due to the fact that the filter's output is a complex function, the filtered image is given by the corresponding magnitude.

F. Feature Extraction Process

In the feature extraction process each ROS image is projected on the real components of the decomposition described by eq. 2, eq. 5 and eq. 6 and the first two moments given by eq. 9. The estimated multi-modal coefficients of the decomposition are used to form the scalar and vector part of a quaternionic representation (eq. 10).

$$q = \left(f_{n,m}^{ART}, \mathbf{v}\right); \quad \mathbf{v} = \left[f_{n,m}^{SH} \quad a_n^{\pm m} \quad f_{n,\mathrm{m}}^{GFB} \right]^T$$

$$a_n^{\pm m} = \frac{n+1}{\pi} \cdot \sum_{n=0}^{\infty} \sum_{\substack{m=-n, \\ n-|m|=even, \\ |m| \le n}}^{+n} I(\rho,\theta) \cdot Z_n^m(\rho,\theta) \quad \text{and} \tag{10}$$

$$f_{n,m}^{GFB} = \left[\mu_{n,m} \quad \sigma_{n,m} \right]^T, \ \forall n,m \in \{1,\ldots \quad \ldots$$

where $a_n^{\pm n}$ are the Zernike moments of $I(\rho,\theta)$, while $\mu_{n,m}$ and $\sigma_{n,m}$ the mean value and standard deviation respectively, for n spatial frequencies and m orientations. The factor $\frac{n+1}{\pi}$ is used to normalize the moment's expression.

The main advantage of using the quaternion representation of the extracted set of features is that the multimodal features can be treated as a quaternion matrix $\mathbf{Q}$ with size $M \times N$, where N denotes the training set of ROS images of our CAD system, while M the total number of the orthonormal basis function.

G. Q-Classifier

Taking into account that $\mathbf{Q}$ contains the features of the N ROS images of the training set, it is clear that each vector quaternion part forms an orthonormal basis - the mammographic image-base. Therefore, if $\mathbf{I}'$ is an unknown ROS image, its projection on each mask for each type of decomposition forms a new quaternion q' (eq. 10). This quaternion q' is identified as normal or abnormal by estimating the minimum distance metric between q' and every element in the quaternion matrix $\mathbf{Q}$.

Thus, the identification problem can be solved by comparing the quaternion of the unknown ROS q' with those contained in matrix $\mathbf{Q}$. The distance between two quaternions corresponds roughly to the distance between orientations as long as the quaternions are fairly close to each other. However, in case of comparing quaternions q and $-q$, even though the distance between them is 2, both have the same orientation. For avoiding this problem, the best way to compare quaternions globally is by using the rotation angle θ between them as metric, given by:

$$\theta = \cos^{-1}\left(2 \cdot \left(\langle q_1 \cdot q_2 \rangle\right)^2 - 1\right) \tag{11}$$

where $\langle q_1 \cdot q_2 \rangle$ denotes the dot product between q_1 and q_2. Quaternions q_1 and q_2 are considered to be unit. Equation 11 follows from the double-angle formula for cosine, considering the fact that the angle between quaternionic orientations is precisely twice the angle between unit quaternions [27]. The rotation angles between quaternion q' and each quaternion of the train in matrix $\mathbf{Q}$, are estimated by:

$$\theta_{i,j}(k) = \underset{i=1}{\overset{N}{И}} \underset{j=1}{\overset{M}{И}} \cos^{-1}\left(2 \cdot \left(\langle q'_{k,i} \cdot \mathbf{Q}_{k,j} \rangle\right)^2 - 1\right) \tag{12}$$

where $i = 1,2,\ldots,N$ is denoting the set of the unknown ROS images, $j = 1,2,\ldots,M$ is denoting the set of the mammographic image-base and with $k = 1,2,\ldots K$ is denoting the total number of the coefficients. The symbol И denotes iteration [28].

Thus, any unknown ROS image $\mathbf{I}'$ is associated with one of the mammographic image-base and recognized as normal or abnormal regarding the column j of matrix $\mathbf{Q}$ that the minimum average rotation angle has occurred.

$$\arg\min_j \left\{ \frac{1}{K} \underset{i=1}{\overset{N}{И}} \underset{j=1}{\overset{M}{И}} \sum_{k=1}^{K} \theta_{i,j}(k) \right\} \tag{13}$$

III. Experimental Results

For our experiments we have used the MIAS MiniMammographic Database [29], provided by the Mammographic Image Analysis Society (MIAS). The database consists of 200-micron pixel edge mammograms with 1024×1024 pixel resolution. In the MIAS Database there are a total of 119 ROS that contain all kinds of existing abnormal tissue. The smallest abnormality extends to 3 pixels in radius, while the largest one to 197 pixels. These 119 ROS along with another 119 randomly selected subimages from entirely normal mammograms were used throughout our experiments. A database of 238 ROSs of 35×35 pixels size is used. The image database has been designed to include all types of different ROS areas abnormalities, i.e. circumscribed, spiculated, ill defined masses, microcalcifications, asymmetry and architectural distortion as well as regions with normal (healthy) tissue.

From a total number of 238 ROS included in the MIAS database, 212 regions are used for the training procedure: 106 groundtruthed abnormal regions along with 106 randomly selected normal ones. In the evaluation procedure, the remaining 26 regions are used that contain 14 groundtruthed abnormal regions together with 12 entirely normal regions. Therefore, no ROS was used both in the training and testing procedure. All classification experiments were performed 10 times using randomly chosen training/testing sets.

A. Q-Classifier

The quaternion matrix $\mathbf{Q}$ is composed by the real components of $V_{n,m}(\rho,\theta)$ (eq.5), of $x_{n,m}(\rho,\theta;\beta)$ (eq.2) and of $Z_n^{\pm m}(\rho,\theta)$ (eq.6) as well as with the first two moments of $g_{f,\theta}(x,y)$ (eq.9); resulting to 36 coefficients per quaternionic

ISBN 978-0-9928626-7-1 © EURASIP 2017

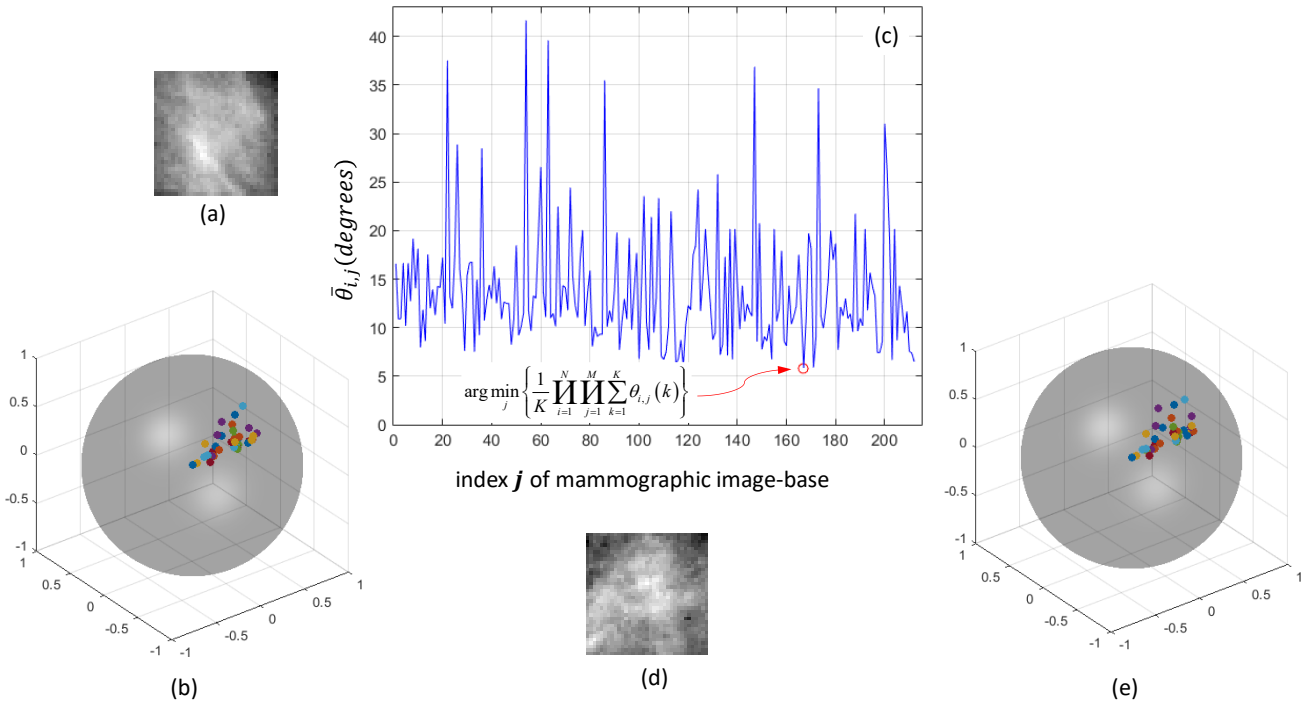

Fig. 1. Identification of a malignant lesion (**a**) the unknown ROS image (**b**) the 3D representation of quaternion feature vector of unknown ROS image (**c**) the average rotational angle between the quaternion and each element of the quaternion matrix **Q** (**d**) the associated ROS image which correspond to the minimum average rotational angle and (**e**) the 3D representation of quaternion feature vector of the associated ROS image

both in the scalar and the imaginary part. The quaternion matrix **Q** defines the image information of all ROS areas used for training. Therefore, each ROS image is described by a quaternion feature vector with 4×36 dimensionality.

In the recognition experiments, the quaternion of the unknown ROS image is projected onto each quaternion in matrix **Q** and the rotation angle in each case is estimated. The unknown ROS image is assigned to the same category (normal or abnormal) with the corresponding index of **Q** that presents the average minimum rotation angle value (eq.13).

B. Discussion

In Fig. 1 one example of identification problem comparing the quaternion feature vector of an unknown ROS image with those contained in matrix **Q** is given. The unknown ROS image is associated with one of the mammographic image-base and recognized as normal or abnormal regarding the column j of matrix **Q** that the minimum average rotation angle has occurred (eq.12 and 13).

The multicolored dots that are depicted on the surface of the unitary sphere correspond to each quaternion feature vector of the unknown ROS image and the associated one of the set of known images. Since the quaternion is unitary, the sphere is also unitary. To depict the feature vector on the sphere, the quaternion is converted to Euler's axis with the appropriate angle using:

$$angle = 2 \cdot \cos^{-1}(s)$$
$$x_{axis} = \frac{x}{\sqrt{1-s^2}},\ y_{axis} = \frac{y}{\sqrt{1-s^2}},\ z_{axis} = \frac{w}{\sqrt{1-s^2}} \qquad (14)$$

where s is the scalar and x, y,w the imaginary parts of the quaternion.

In our experiments the training set is randomly formed consisting of 212 ROS images (106 normal and 106 abnormal) from the MIAS database. The normal regions are randomly chosen from normal mammograms with all different types of tissue, while the abnormal regions are selected to include all different kind of abnormalities. The testing set is formed using the remaining 26 ROS images (12 normal and 14 abnormal) including all different types of tissue. All classification experiments are performed 10 times using randomly chosen training/testing sets and the mean identification accuracy is obtained. The identification results of the ROS are presented by measuring the Area Under the Curve (AUC) which equals to 0.934. The ROC curve in Fig. 2 shows the relative trade-offs between benefits (true positives) and costs (false positives). It is clear that the closer the ROC curve follows the left-hand and the top border of the ROC space the more accurate the classification result will be. In our experiments, a quantitative comparison of the proposed feature extraction and classification method's accuracy is also presented compared with analogous results in our previous work in [11]. In comparison to the non-linear classifier techniques in [11], the proposed Q-classifier with the multi-modal feature descriptors present similar recognition accuracy results (0.934 compared to 0.929 and 0.851 in [11] respectively), with smaller computational cost and higher diagnosis speed at the same time.

IV. Conclusions

In this paper we have presented a new CAD system for the automatic identification of all types of lesions in digital mammograms. The proposed system consists of two main modules:

ISBN 978-0-9928626-7-1 © EURASIP 2017

The feature extraction module, where multi-modal features from Regions of Suspicion are extracted using a new feature extraction technique based on the decomposition of ROS into a set of localized basis functions with different shapes (Shapelets, ART, Zernike moments, Gabor filters). In the second Classification module, the fused features are used in quaternionic representation and are diagnosed as belonging to normal or abnormal tissue. Experimental results have shown that the proposed multi-modal feature set used with the Q-classifier, performs better than unimodal feature sets used in similar problems in the literature. Future work will address the problem of specific type of cancer identification (speculated, ill-defined, architectural, amorphous microcalcifications) using the same multi-modal feature extraction technique and the classifier scheme to build a CAD system that will serve as a double-reading aid, thus reducing reading errors that are pruned to be committed especially by junior radiologists and resulting in diagnostic accuracy improvement for radiologists.

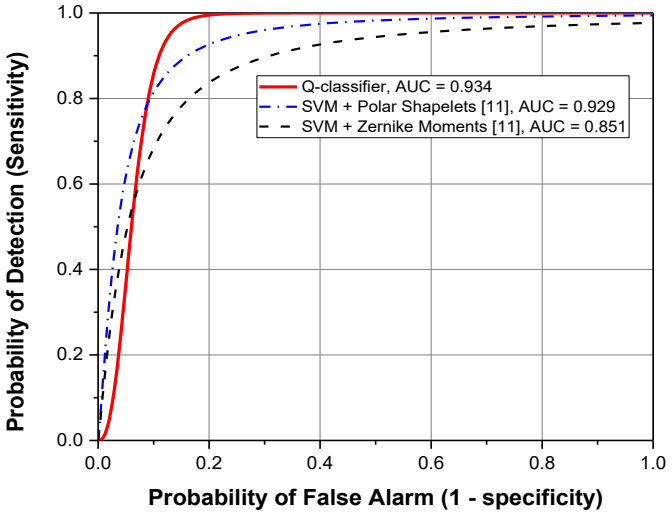

Fig. 2. The ROC curve of the proposed method

REFERENCES

[1] Ferlay, J., Soerjomataram, I., Dikshit, R., Eser, S., Mathers, C., Rebelo, D.M. Parkin, D. Forman & Bray, F. (2015) Cancer incidence and mortality worldwide: sources, methods and major patterns in GLOBOCAN 2012, International Journal of Cancer, 136(5), E359-E386.

[2] Bird, R. E., Wallace, T. W., & Yankaskas, B. C. (1992) Analysis of cancers missed at screening mammography, Radiology, 184(3), pp 613-617.

[3] Kerlikowske, K., Carney, P. A., Geller, B., Mandelson, M. T., Taplin, S. H., Malvin, K., Ernster V, Urban N, Cutter G, Rosenberg R, Ballard-Barbash R. (2000) Performance of screening mammography among women with and without a first-degree relative with breast cancer, Annals of Internal Medicine, 133(11), pp 855-863.

[4] Miranda, G. H. B., & Felipe, J. C. (2014) Computer-aided diagnosis system based on fuzzy logic for breast cancer categorization, Computers in biology and medicine.

[5] Dheeba, J., Singh, N. A., & Selvi, S. T. (2014) Computer-aided detection of breast cancer on mammograms: A swarm intelligence optimized wavelet neural network approach, Journal of biomedical informatics, 49, pp 45-52.

[6] Varela, C., Tahoces, P. G., Méndez, A. J., Souto, M., & Vidal, J. J. (2007) Computerized detection of breast masses in digitized mammograms, Computers in Biology and Medicine, 37(2), pp 214-226.

[7] Meenalosini, S., & Janet, J. (2012) Computer aided diagnosis of malignancy in mammograms, European Journal of Scientific Research, 72(3), pp 360-368.

[8] Oliver, A., Torrent, A., Llado, X., & Marti, J. (2010) Automatic diagnosis of masses by using level set segmentation and shape description, In Pattern Recognition (ICPR), 2010 20th International Conference on pp 2528-2531, IEEE.

[9] Mousa, R., Munib, Q., & Moussa, A. (2005) Breast cancer diagnosis system based on wavelet analysis and fuzzy-neural, Expert systems with Applications, 28(4), pp 713-723.

[10] Moayedi, F., Azimifar, Z., Boostani, R., & Katebi, S. (2010) Contourlet-based mammography mass classification using the SVM family, Computers in biology and medicine, 40(4), pp 373-383.

[11] Apostolopoulos, G., Koutras, A., Christoyianni, I., and Dermatas, E. (2014) Computer Aided Classification of Mammographic Tissue Using Shapelets and Support Vector Machines, In Artificial Intelligence: Methods and Applications, pp 510-520, Springer International Publishing.

[12] Hamilton, W. R. (1844) On a new species of imaginary quantities connected with a theory of quaternions, In Proceedings of the Royal Irish Academy, pp 424-434.

[13] Sun, Y., Chen, S., & Yin, B. (2011) Color face recognition based on quaternion matrix representation, Pattern Recognition Letters, 32(4), pp 597-605.

[14] Chen, B. J., Shu, H. Z., Zhang, H., Chen, G., Toumoulin, C., Dillenseger, J. L., & Luo, L. M. (2012) Quaternion Zernike moments and their invariants for color image analysis and object recognition, Signal Processing, 92(2), pp 308-318.

[15] Hanson, A. J. (2005) Visualizing quaternions, In ACM SIGGRAPH Courses, ACM.

[16] Refregier, A. (2003) Shapelets—I. A method for image analysis. Monthly Notices of the Royal Astronomical Society, 338(1), pp 35-47.

[17] M. Bober, Mpeg-7 visual shape descriptors, IEEE Trans. Circuits Syst. Video Technol., vol. 1(6), June 2001.

[18] S. Jeannin, Mpeg-7 Visual part of experimentation Model Version 9.0, in ISO/IEC JTC1/SC29/WG11/N3914, 55th Mpeg Meeting, Pisa, Italia, Jan. 2001.

[19] W. Y. Kim and Y.-S. Kim, A new region-based shape descriptor, in TR 15-01, Pisa, Dec. 1999.

[20] F. Zernike, Diffraction theory of the cut and its improved form, the phase contrast method, Physica, Vol. 1, pp. 689-704, 1934

[21] C. Teh, R. Chin, On image analysis by the methods of moments, IEEE Trans. Pattern Anal. Mach. Intell., Vol. 10, pp. 496-513, 1988.

[22] R. Bailey and M. Srinath, Orthogonal moment feature for use with parametric and non-parametric classifiers, IEEE Trans. Pattern Anal. Mach. Intell., Vol. 18, 1988.

[23] A. Khotanzad and Y. Hong, Classification of invariant image representations using a neural network, IEEE Trans. Acoust. Speech Signal Processing, Vol. 38, pp. 1028-1038, 1990.

[24] Tahmasbi, A., Saki, F., & Shokouhi, S. B.: Classification of benign and malignant masses based on Zernike moments. Computers in biology and medicine, 41(8), 726-735 (2011).

[25] J. G. Daugman, Uncertainty Relation for Resolution in Space, Spatial Frequency, and Orientation Optimized by Two-Dimensional Visual Cortical Filters, Journal of Optical Society America A, Vol. 2, No. 7, 1985, pp. 1160 - 1169.

[26] T. Andrysiak, and M. Choras, Image retrieval based on hierarchical Gabor filters, International Journal of Mathematics and Computer Science, Vol. 15, No. 4, 2005, pp. 471-480

[27] Huynh, D. Q. (2009) Metrics for 3D rotations: Comparison and analysis, Journal of Mathematical Imaging and Vision, 35(2), pp 155-164.

[28] V. Salov, Notation for Iteration of Functions, Iteral, arXiv preprint arXiv:1207.0152 (2012).

[29] MIAS at http://peipa.essex.ac.uk/info/mias.html

ISBN 978-0-9928626-7-1 © EURASIP 2017